materials

MDPI

Article

Comparison between Mechanical Properties and Joint Performance of AA 2024-T351 Aluminum Alloy Welded by Friction Stir Welding, Metal Inert Gas and Tungsten Inert Gas Processes

Miodrag Milčić [1], Damjan Klobčar [2], Dragan Milčić [1], Nataša Zdravković [1], Aleksija Đurić [3] and Tomaž Vuherer [4,*]

[1] Faculty of Mechanical Engineering, University of Nis, Aleksandra Medvedeva 14, 18000 Niš, Serbia; miodrag.milcic@masfak.ni.ac.rs (M.M.); dragan.milcic@masfak.ni.ac.rs (D.M.); natasa.zdravkovic@masfak.ni.ac.rs (N.Z.)
[2] Faculty of Mechanical Engineering, University of Ljubljana, Aškerčeva 6, 1000 Ljubljana, Slovenia; damjan.klobcar@fs.uni-lj.si
[3] Faculty of Mechanical Engineering, University of East Sarajevo, Vuka Karadžića 30, 71123 Sarajevo, Bosnia and Herzegovina; aleksija.djuric@ues.rs.ba
[4] Faculty of Mechanical Engineering, University of Maribor, Smetanova 17, 2000 Maribor, Slovenia
* Correspondence: tomaz.vuherer@um.si

Abstract: The aim of this work is to study joining Al 2024-T3 alloy plates with different welding procedures. Aluminum alloy AA 2024-T351 is especially used in the aerospace industry. Aluminum plates are welded by the TIG and MIG fusion welding process, as well as by the solid-state welding process, friction stir welding (FSW), which has recently become very important in aluminum and alloy welding. For welding AA2024-T35 with MIG and TIG fusion processes, the filler material ER 4043—$AlSi_5$ was chosen because of reduced cracking. Different methods were used to evaluate the quality of the produced joints, including macro- and microstructure evaluation, in addition to hardness and tensile tests. The ultimate tensile strength (UTS) of the FSW sample was found to be 80% higher than that of MIG and TIG samples. The average hardness value of the weld zone of metal for the MIG- and TIG-produced AA2024-T3511 butt joints showed a significant decrease compared to the hardness of the base metal AA2024-T351 by 50%, while for FSW joints, in the nugget zone, the hardness is about 10% lower relative to the base metal AA2024-T3511.

Keywords: AA2024-T351; friction stir welding (FSW); tungsten inert gas (TIG); metal inert gas (MIG); mechanical properties

Citation: Milčić, M.; Klobčar, D.; Milčić, D.; Zdravković, N.; Đurić, A.; Vuherer, T. Comparison between Mechanical Properties and Joint Performance of AA 2024-T351 Aluminum Alloy Welded by Friction Stir Welding, Metal Inert Gas and Tungsten Inert Gas Processes. *Materials* **2024**, *17*, 3336. https://doi.org/10.3390/ma17133336

Academic Editor: Frank Czerwinski

Received: 22 May 2024
Revised: 18 June 2024
Accepted: 2 July 2024
Published: 5 July 2024

1. Introduction

Aluminum constructions find frequent applications in various transportation sectors, notably in automotive engineering, railway vehicle manufacturing [1], ship construction, aviation [2], and space technology, thanks to the favorable mechanical properties and lightweight nature of aluminum alloys. The welded assemblies of automobiles, locomotives, marine vessels, aircraft, and spacecraft, comprised of diverse aluminum alloys, are primarily interconnected using fusion welding methods such as metal inert gas (MIG) [3,4] and tungsten inert gas (TIG) welding [5].

The fusion welding techniques adeptly bond materials with favorable weldability characteristics, defined by the ability to create defect-free welded joints. The weldability of aluminum alloys is influenced by various factors including their affinity to oxygen, high thermal expansion and conductivity, significant shrinkage upon solidification, and notable hydrogen solubility in the liquid phase, a trait that diminishes considerably during the solidification process. By welding aluminum alloys, the mechanical properties

and resistance to corrosion in the HAZ decrease; porosity, hardening and solidification cracks appear. Aluminum alloys are welded with additional material with increased Si or Mg content. The appearance of defects in the area of welded metal is also affected by poorly prescribed technology of the welding procedure, which reduces the reliability of the welded structure. Remarkably, the typical imperfections associated with traditional welding methods, including solidification cracking, oxidation, distortion, and porosity, are absent in friction stir welding (FSW) applications [6–8].

FSW is a solid-state welding process that uses the heat generated between the tool and base metals. FSW shows various advantages over the fusion welding process [9,10], such as reducing manufacturing time and minimal deformation and distortion of the joints [11]. In the last 20 years, friction stir welding has been increasingly applied to weld various aluminum alloys [12–15].

Laser and electron beam welding are used to weld parts of light structures made of aluminum alloys [16].

Aluminum alloy 2024, which is known for age-hardening, is part of the 2XXX series of alloys where copper is the primary alloying element. These alloys achieve mechanical properties that can be comparable to carbon steels due to the formation of $CuAl_2$ particles during natural or artificial aging processes. Despite their excellent strength, these alloys exhibit poor corrosion resistance, which is why they are often coated with pure aluminum to enhance their corrosion protection. They are predominantly employed in the aviation industry owing to their high strength and excellent fatigue characteristics. Additionally, the incorporation of elements like magnesium and lithium reduces the specific density and enhances the performance of aluminum alloys for aerospace applications [17].

Typically, 2XXX series alloys exhibit poor weldability when using fusion welding techniques such as MIG or TIG due to their high susceptibility to cracking. Consequently, friction stir welding (FSW) is predominantly utilized for joining these alloys [18,19]. This study presents a comparative analysis of the structural and mechanical properties of butt-welded joints produced by MIG, TIG, and FSW methods. The mechanical properties of MIG and TIG joints were compared with those of FSW joints fabricated under optimal parameters [18,19]. The evaluation of the quality of the welded joints was conducted through visual inspection, macro- and microstructural analysis, hardness measurements of the welded joint, and tensile property testing.

2. Materials and Methods

2.1. Material

AA2024-T351 aluminum alloy rolled sheets were welded in a butt-joint configuration using TIG, MIG, and FSW techniques. The 8 mm thick AA2024-T351 sheets were cut into plates measuring 300 mm in length and 125 mm in width for welding with the aforementioned techniques. The chemical and mechanical properties of the AA2024-T351 alloy, based on standard specifications, are provided in Tables 1 and 2.

Table 1. Chemical properties of base material AA 2024-T351.

Alloying Element	Mn	Fe	Mg	Si	Cu	Zn	Ti	Al
wt.%	0.65	0.17	1.56	0.046	4.7	0.11	0.032	Balance

Table 2. Mechanical properties of base material AA 2024 T351.

Yield Strength *YS* (MPa)	Ultimate Tensile Strength *UTS* (MPa)	Elongation at Break *E* (%)	Hardness HV
370	481	17.9	137

2.2. Fusion Welding of AA2024-T351

The AA2024-T351 plates were fusion-welded using two different techniques: TIG and MIG welding processes. The TIG arc was shielded with argon gas (ISO 14175-I1-Ar 5.0), while the MIG arc was shielded with a gas mixture of Argon + He (ISO 14175-I3-ArHe-30). In this experiment, a Fronius Transpuls Synergic 4000 direct-current electrode-positive (DCEP) MIG welding machine and a Fronius Magic Wave 4000 Job G/F direct-current electrode-negative (DCEN) TIG welding machine (Fronius, Wels, Austria) were used in producing the welds. The chemical properties of the filler material used during welding are given in Table 3.

Table 3. Chemical composition of the filler material of wire EN ISO 18273 [20] S Al 4043A ($AlSi_5$).

Element	Mn	Fe	Mg	Si	Cu	Zn	Ti	Be	Al
wt.%	<0.15	<0.6	<0.2	4.5–5.5	<0.3	<0.1	<0.15	<0.0003	Balance

The welding parameters for MIG and TIG butt welding of aluminum alloy 2024-T351 are provided in Table 4, where the parameter η is thermal efficiency.

Table 4. Welding parameters for the MIG butt joint welding process.

Welding Process	Run	Current I (A)	Voltage U (V)	Welding Speed v (cm/min)	Heat Input H = I·U·η/v (J/mm)
MIG	1	155	21.7	41.88	385
	2	180	23.2	52.92	379
	3	170	22.7	49.98	371
TIG	1	230	12.9	11.55	1233
	2	240	11.7	17.93	751.3
	3	200	12.6	12.09	998
	4	200	13.3	20.47	624

2.3. FSW of AA2024-T351

FSW of AA2024-T351 was carried out using a conventional vertical milling machine (Figure 1a). The welding tool had a tapered threaded cylindrical shape, with its dimensions and geometry displayed in Figure 1b. The FSW tool was made from $55CrMo_8$ tool steel and was heat-treated to achieve a hardness of 50 HRC.

(**a**) (**b**)

Figure 1. (**a**) Conventional milling machine for FSW and (**b**) geometry of FSW tool.

The dimensions of the welding samples were 500 mm × 65 mm × 6 mm. Before welding, an austenitic plate was utilized as the base plate under the welding plate. The length of the weld was approximately 400 mm.

The most critical parameters in FSW are the welding speed and the tool's rotational speed. Experimental research was conducted with a constant tool rotational speed, while varying the welding speed (Table 5).

Table 5. Friction stir welding parameters [18,19].

Sample	Rotation Rate n rpm	Welding Speed v mm/min	Ratio n/v rev/mm
A-I	750	73	10.27
B-II		116	6.47
C-III		150	5

By investigating the mechanical properties of joints welded through FSW for the welding parameter of the number of revolutions of the tool/welding speed (n/v), A-I (750/73), B-II (750/116), and C-III (750/150), the optimal parameters were found: tool speed n = 750 rpm and welding speed v = 116 mm/min [18,19]. In the following, a comparison of the mechanical and structural properties of butt welds made by MIG and TIG welding will be compared with FSW welds made with welding parameters n = 750 rpm and v = 116 mm/min.

2.4. Characterization of AA2024-T351 Welds

Test specimens for macro- and microstructural analysis, including tensile testing and hardness testing, were prepared from the welded samples by water jet cutting. The microstructure was investigated on the cross-section of the samples following standard metallographic preparation and etching with Keller's reagent. A Leica Q500MC optical microscope (LM) (Leica, Wetzlar, Germany) was utilized to analyze the microstructure of the welded joint. Additionally, tests were conducted using a JOEL JSM-6610LV scanning electron microscope (SEM) (JOEL, Tokyo, Japan).

The Vickers hardness measurement of MIG and TIG welded joints was performed on a Willson VH1150 hardness measuring device (Buehler, Lake Bluff, IL, USA). According to the standard procedure, hardness measurements were made along two horizontal directions near the butt and near the root of the weld with three hardness measurements each in the base metal (BM), three in the heat-affected zone (HAZ), and three in the weld metal (WM). Figure 2 show the arrangement of hardness measurement points in tested welded joints. Measurement points are marked with numbers 1–30 and apply to MIG and TIG welded joints.

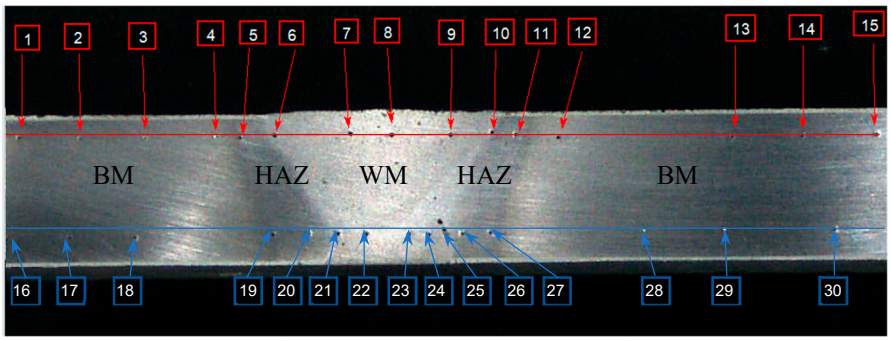

Figure 2. Hardness measurement points of the joint.

Vickers hardness measurement of joints welded through FSW was conducted using the HVS-1000 micro Vickers hardness tester (TIME, Beijing, China). The hardness profile was analyzed along three horizontal directions: the weld face (1 mm from the face of the welded joint), the weld center (3 mm from the face of the welded joint), and the weld root

(5 mm from the face of the welded joint) (Figure 3). The distance between the indentations was 0.5 mm.

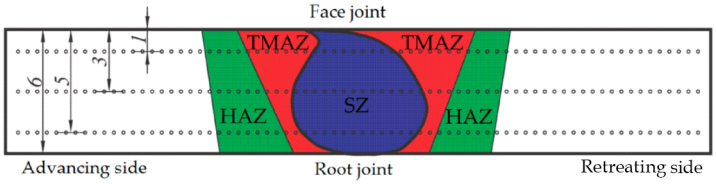

Figure 3. Microhardness measurement scheme with characteristic zones of welded joint (SZ—stir zone, TMAZ—thermomechanically affected zone, HAZ—heat-affected zone).

Tensile properties were assessed at room temperature using a Shimadzu AG-X 300 kN tensile tester (Shimadzu, Kyoto, Japan). Test specimens, defined by the ASTM E8M standard [21] and obtained from welded samples perpendicular to the weld joint, were employed. Specimens were cut from the welded samples using the water jet cutting process.

3. Results and Discussion

3.1. Visual Inspections

Following the welding processes, the welded samples were evaluated through visual inspection, metallographic tests, Vickers hardness tests, and tensile tests to compare the effects of the welding processes on the quality of joining 8 mm AA2024-T351 in similar butt welds.

Figure 4 illustrates the face side of a welded joint. The welded joint was made with a backing material (Figure 4a,b).

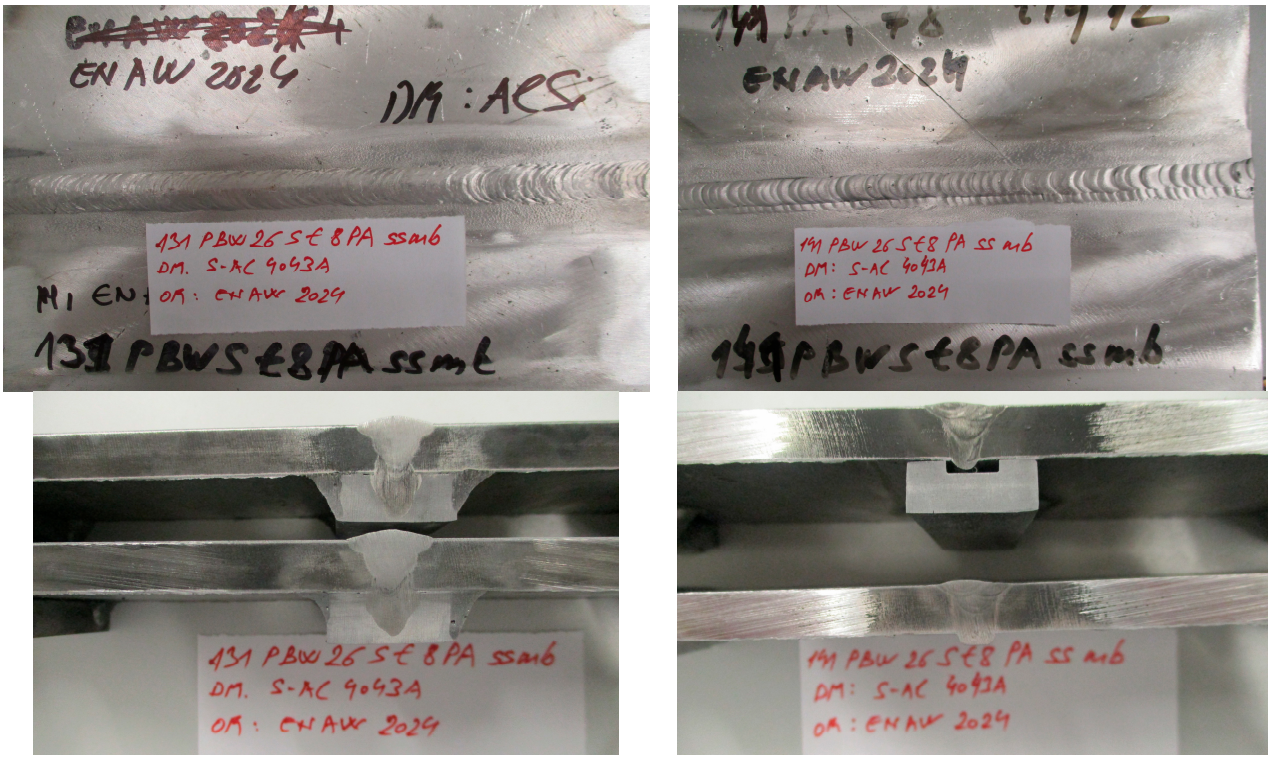

(**a**) (**b**)

Figure 4. *Cont.*

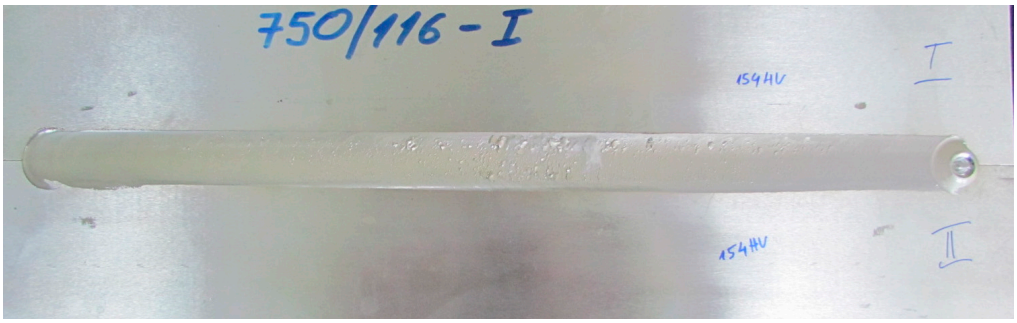

(c)

Figure 4. Face side of the welded joint with (**a**) MIG; (**b**) TIG; (**c**) FSW process.

3.2. Macro- and Microscopic Examinations

Figure 5 presents the macrostructure of the AA 2024-T351 butt joints, welded using FSW (Figure 5a–c), MIG (Figure 5d), and TIG (Figure 5e) techniques, observed on the cross-section of the weld axis. In the FSW joins, there are no defects such as tunnels or cracks. The MIG and TIG joint has a regular symmetrical shape without apparent defects such as cracking, undercutting, and porosity.

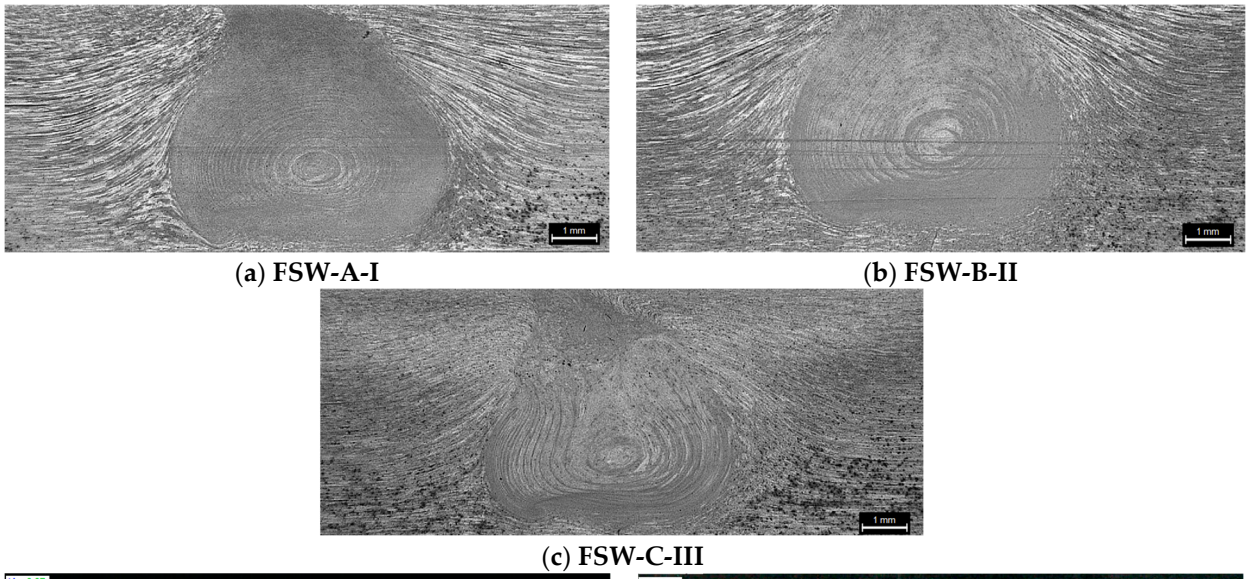

(a) FSW-A-I **(b) FSW-B-II**

(c) FSW-C-III

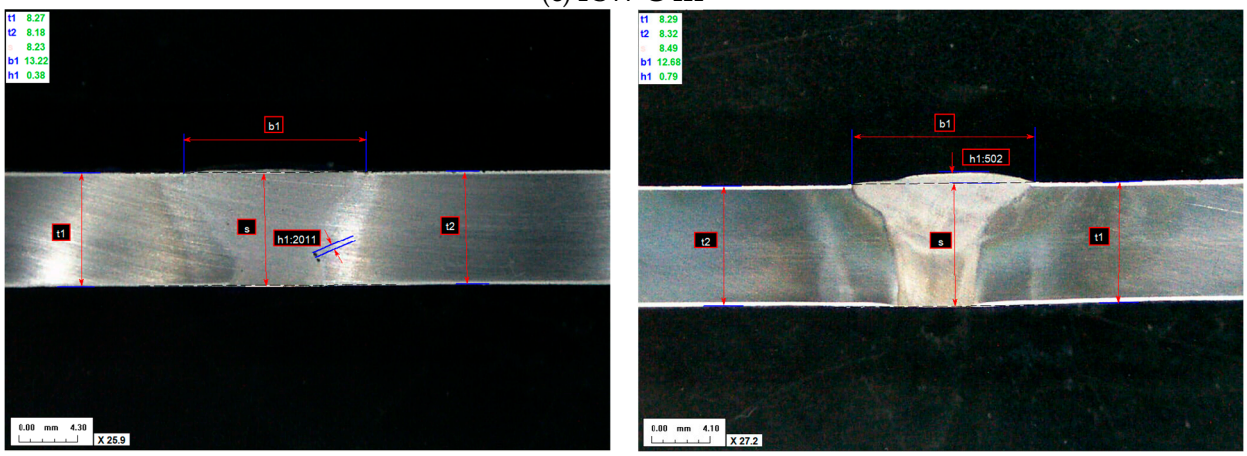

(d) MIG **(e) TIG**

Figure 5. Macrostructure of a welded joint.

The macrostructure of FSW welds clearly indicates three characteristic zones: the stirred zone (SZ), the thermomechanically affected zone (TMAZ), and the heat-affected zone (HAZ). Also, in MIG and TIG welded joints, characteristic zones are observed: the weld metal zone (WM) and the heat-affected zone (HAZ). The heat-affected zone (HAZ) of the TIG welded joint is wider than the heat-affected zone of the MIG welded joint, due to the greater amount of heat input.

The microstructure of the MIG welded joint is given in Figure 6.

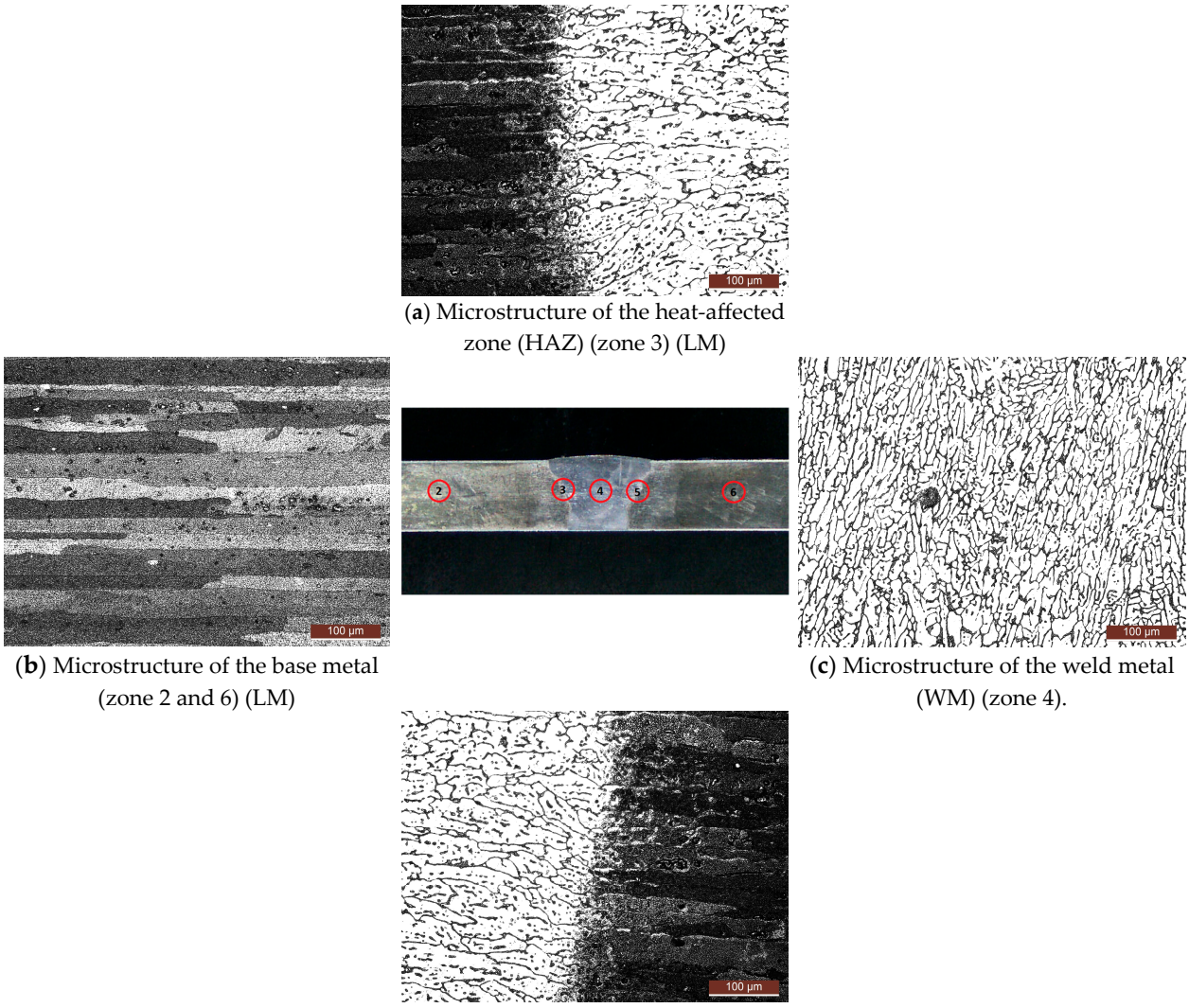

(**a**) Microstructure of the heat-affected zone (HAZ) (zone 3) (LM)

(**b**) Microstructure of the base metal (zone 2 and 6) (LM)

(**c**) Microstructure of the weld metal (WM) (zone 4).

(**d**) Microstructure of the heat-affected zone (HAZ) (zone 5).

Figure 6. Appearance of cross-section of the specimen with view of microscopic examination zones—MIG [22].

For the microstructure of the zone between the HAZ and the weld metal (WM) (zone 3–Figure 6a), precipitate particles are observed in the weld metal up to the HAZ, separated by the grain boundaries and in the grain to a certain extent with a narrow columnar orientation. In HAZ, particles of intermetallic phases (IMPs) are separated by grain boundaries, and larger IMP particles are also present. In the microstructure of the weld metal (zone 4—Figure 6c), precipitate particles separated by the grain boundaries, and, in places, also in the grain, can be observed. The grains are of different sizes and have a dendritic orientation.

Figure 7 shows the EDS analysis of zones 3 and 4 (Figure 6a). Table 6 shows the results of the element concentration percentages.

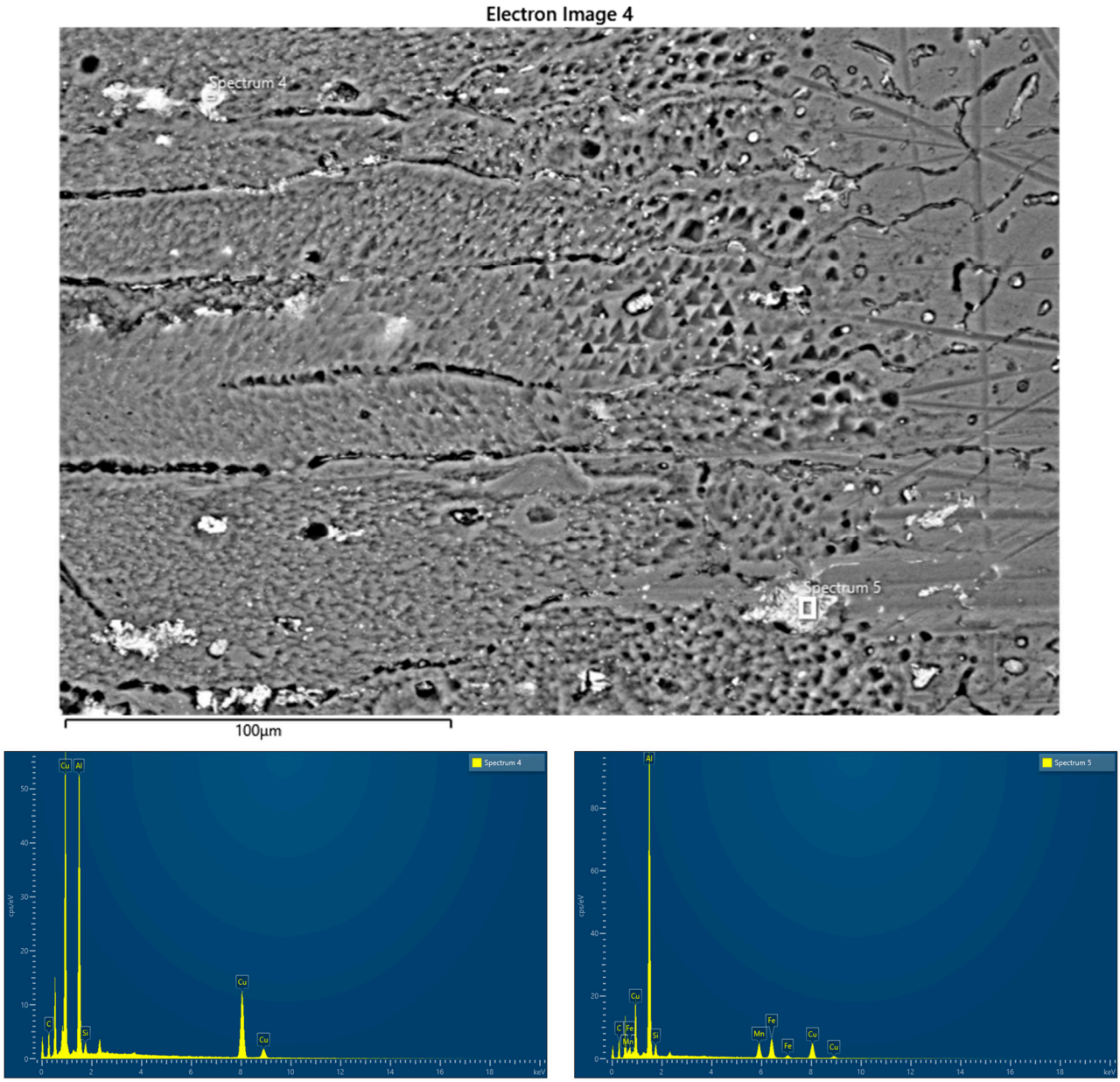

Figure 7. EDS spot analysis of MIG joint sample (SEM).

Table 6. Elements' concentrations for MIG joint sample (%).

Spectrum Label	Spectrum 4	Spectrum 5
Al	42.78	55.23
Si	2.15	3.23
Mn		8.64
Fe		12.68
Cu	55.07	20.21
Total	100.00	100.00

Single precipitates were analyzed with EDS to determine their chemical composition. EDS analysis was performed on two different points of the weld metal zone (WM) and heat-affected zone (HAZ). In point 4 (the silverish spot), the atomic percentage of the element Cu is 55% (highest), the atomic percentage of the element Al is 43% (second highest), and that of Si is 2.15%. Therefore, point 4 has the element Cu as the majority element for the silvery spot, possibly from the AA2024 parent metal. In point 5, the atomic percentage of

the element Al is 55% (highest), the atomic percentage of the element Cu is 20.2% (second highest), that of Fe id 13% (third highest), that of Mn is 8.6% (fourth highest), and that of Si is 3.23%. It was found that point 4 consists of the Fe_mAl_n compound, and the Cu element was normally found as the alloying element for AA2024.

The microstructure of the TIG welded joint is given in Figure 8.

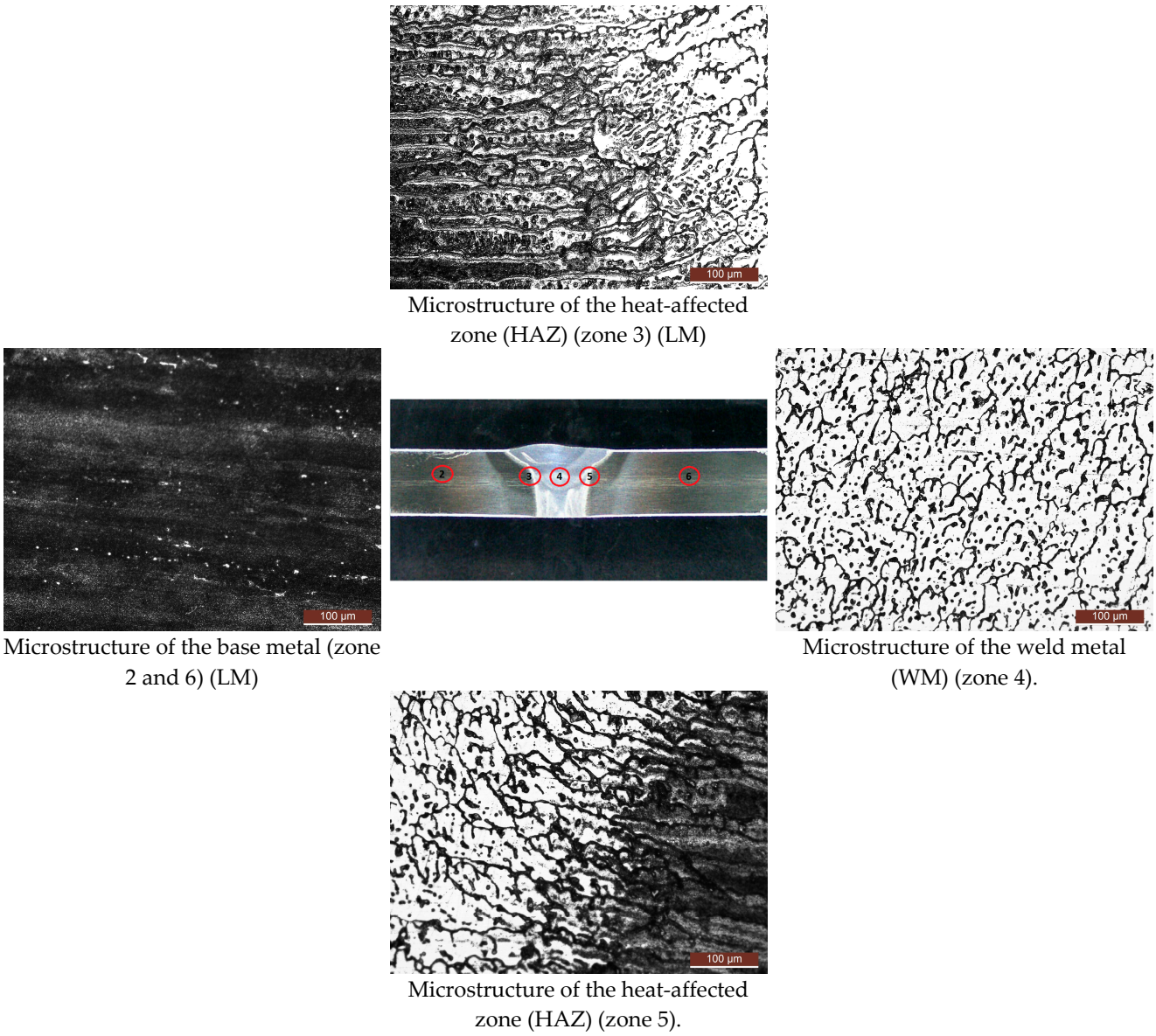

Microstructure of the heat-affected zone (HAZ) (zone 3) (LM)

Microstructure of the base metal (zone 2 and 6) (LM)

Microstructure of the weld metal (WM) (zone 4).

Microstructure of the heat-affected zone (HAZ) (zone 5).

Figure 8. Appearance of cross-section of the specimen with view of microscopic examination zones—TIG.

The microstructure of the base material AA2024-T351 (zones 2 and 6) has an elongated grain in the rolling direction with separated large particles of IMP precipitate. In the microstructure of the zone between the weld metal and HAZ (zone 3 and 5), sediment particles can be observed at the boundaries and inside the grain, and the grain has an orientation in the direction of rolling. In the microstructure of the weld metal zone, sediment particles of different sizes are observed at the boundaries and in the grain itself. The grain has a dendritic orientation. Figure 9 shows different points of the TIG welded sample and Table 7 shows the results of the element concentration percentages.

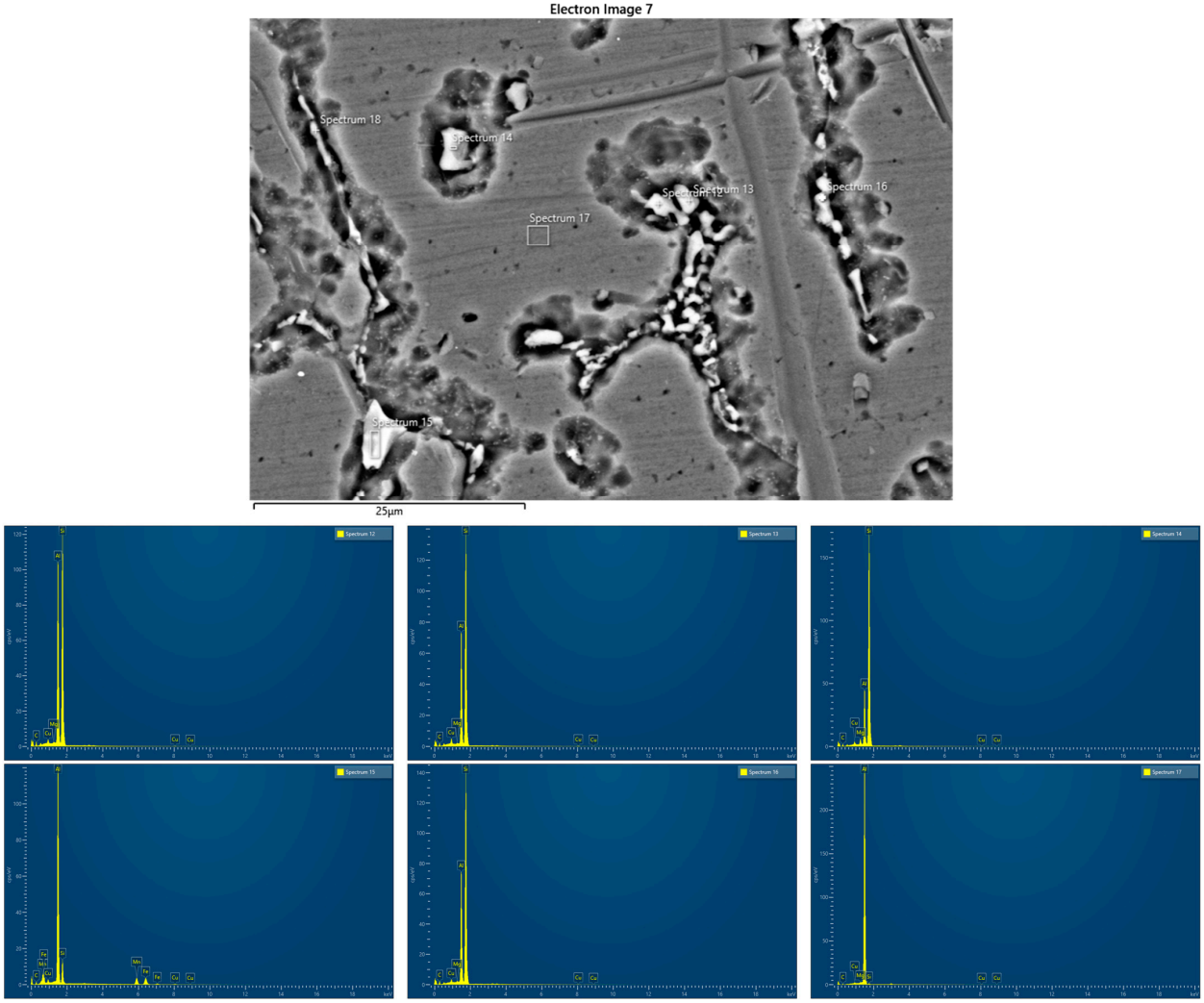

Figure 9. EDS spot analysis of TIG joint sample (SEM).

Table 7. Elements' concentrations for TIG joint sample (%).

Spectrum Label	Spectrum 12	Spectrum 13	Spectrum 14	Spectrum 15	Spectrum 16	Spectrum 17
Mg	0.18	0.21	1.49		0.23	0.20
Al	35.65	26.70	16.09	59.44	26.66	98.10
Si	62.48	70.24	80.71	9.98	71.38	0.98
Mn				12.94		
Fe				15.07		
Cu	1.68	2.85	1.72	2.56	1.72	0.71
Total	100.00	100.00	100.00	100.00	100.00	100.00

EDS analysis was performed on five different points of the weld metal zone. Point 17 is the main matrix, and the amount of Al measured is high. In points 12, 13, 14, and 16 (the silverish spot), the atomic percentage of the element Si is between 62% and 81% (highest), the atomic percentage of the element Al is between 16 and 35% (second highest), that of Cu is between 0.74% and 1.27%, and that of Mg is between 0.21% and 1.72%. It was shown that in points 12, 13, 14, and 16, Al-Si is an alloy from ER4043, which is from the Al-Si alloy group. The atomic percentages of Cu and Mg elements in WM were relatively high due to the IMC (intermetallic compound) interaction that occurred during the solidifying process, and this produced Al_mCu_n and Al_mMg_n compounds. It was found that in this region, the elements from a parent metal such as Cu and Mg were solidified together with

the elements presented in the weld metal, producing IMCs. In point 15, the content of Al is 59.4% (highest), that of Fe is 15% (second highest), Mn is 13% (third highest), Si is 10% (fourth highest), and Cu is 2.6%. The atomic percentages of Fe and Mn elements in WM were relatively high due to the IMC interaction that occurred during the solidifying process, and this produced Al_mFe_n and Al_mMn_n compounds.

The microstructure of the FSW welded joint is given in Figure 10.

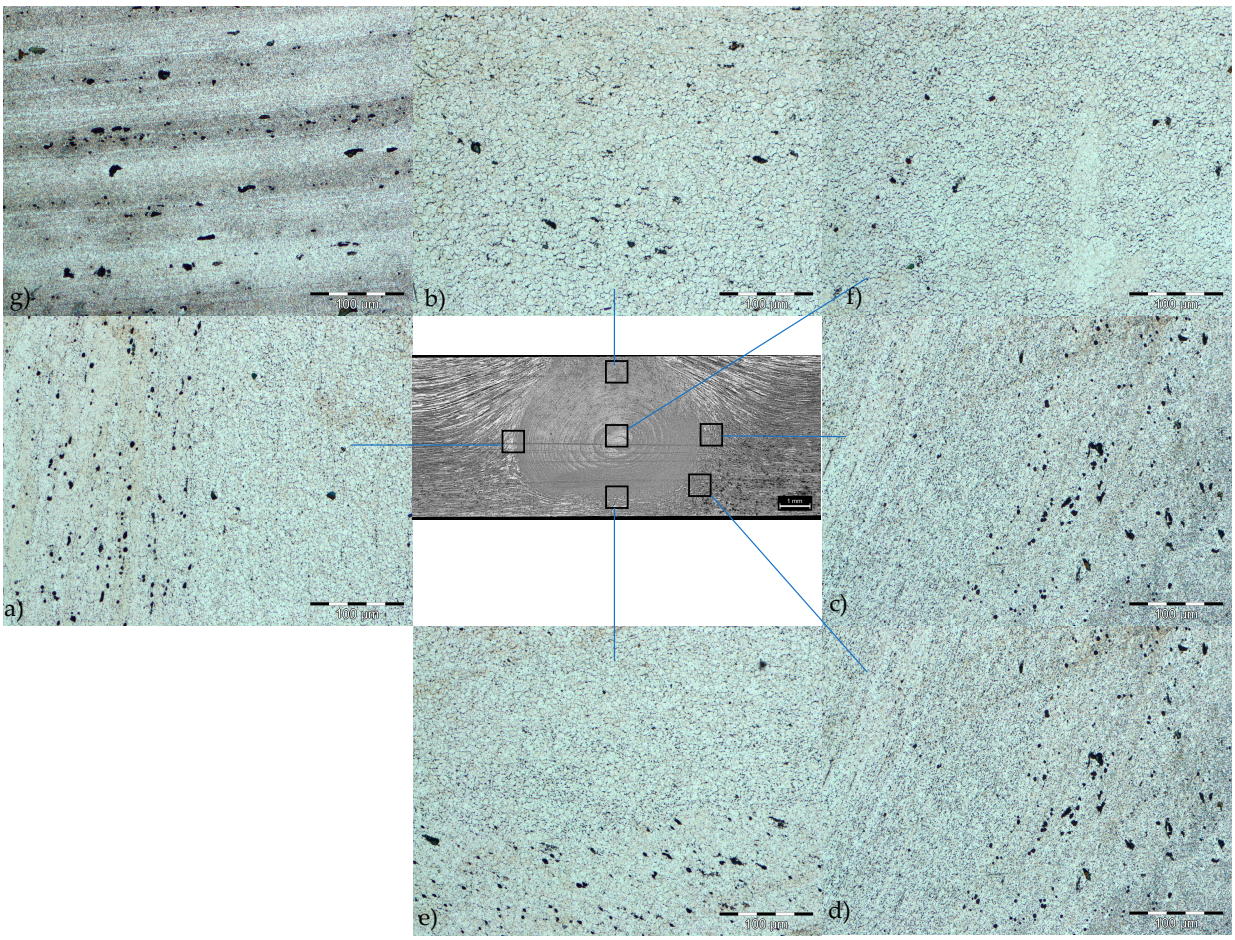

Figure 10. The microstructure of FSW joint: (**a**–**e**) interface between the SZ and the TMAZ; (**f**) SZ; (**g**) BM.

The HAZ is poorly defined. In different areas of the joint (Figure 10a–e) of the thermomechanically affected zone (TMAZ), grains of different sizes and orientations were obtained. The grain size in the TMAZ decreases towards the nugget region. The structure in the nugget (stir zone) is very fine-grained. A significant number of dark spots, which are sediment particles, can be observed in the TMAZ. The microstructure of the nugget is characterized by very small, equiaxed grains (Figure 10f), which is attributed to dynamic recrystallization.

3.3. Tensile Testing

Tensile tests were conducted on specimens cut from AA2024-T351 welds created using TIG, MIG, and FSW techniques. These tests aimed to determine tensile properties such as ultimate tensile strength (UTS), yield strength (YS), and elongation (E%). The tensile test results are given in Table 8. The place of fracture of the tested specimens obtained by all welding procedures are in the weld metal for TIG and MIG welded specimens, i.e., in the stir zone for the FSW specimen.

Table 8. Tensile test results of welded joints.

Welding Process	Yield Strength *YS* (MPa)	Ultimate Tensile Strength *UTS* (MPa)	Elongation at Break *A* (%)	Joint Efficiency %
MIG	209	261	1.3	54
TIG	145	263	5.2	55
FSW	336.6	469.09	7.2	97

The comparative results of the tension test are shown in Figure 11.

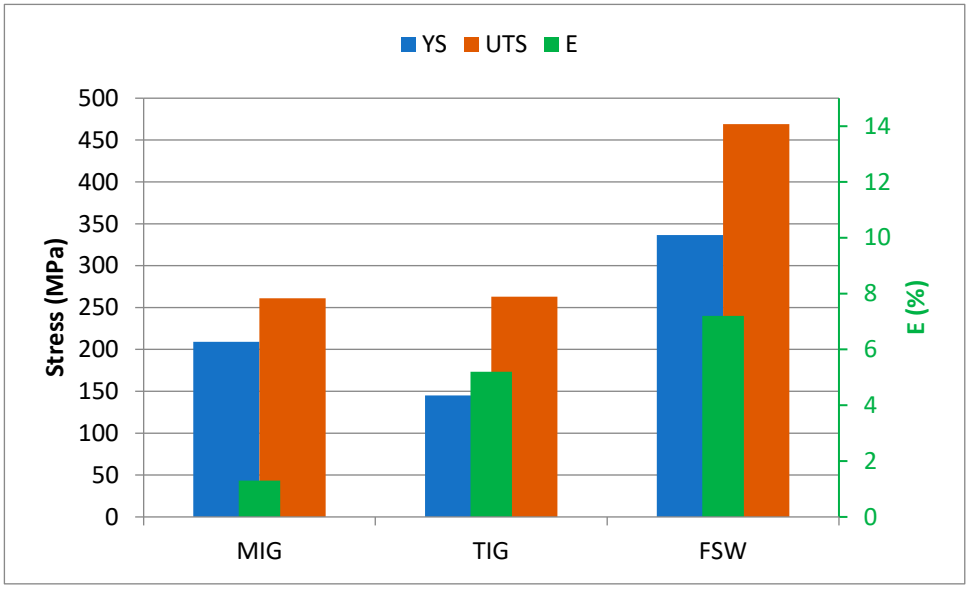

Figure 11. Ultimate tensile strength, yield strength, and elongation percentage of the similar AA2024-T351 butt joints welded using different techniques.

It was found that the tensile properties (UTS and YS) and percentage elongation (E) of the welded tensile specimens by friction stir welding are better than the properties of the welded tensile specimens obtained by conventional welding methods, i.e., TIG and MIG welding [23–25]. The joint efficiency, which is the ratio of the tensile strength of the welded joint to the tensile strength of the base metal, is 97% for friction stir welding compared to 54% and 55%, respectively, for the MIG and TIG welding processes.

3.4. Hardness Distribution

Figure 12 shows the Vickers hardness profile of the cross-section of MIG and TIG welded joints measured near the weld face, while Figure 13 shows the hardness profile of MIG and TIG welded joints measured near the root of the weld. For an MIG welded joint, the average hardness in the weld metal zone near the weld face is 88 ± 5.5 HV, and for a TIG welded joint, the average hardness in the weld metal zone near the weld face is 68 ± 7.7 HV. For the MIG welded joint, the average hardness in the weld metal zone near the weld root is 94 ± 1.5 HV, and for the TIG welded joint, the average hardness in the weld metal zone near the weld root is 69 ± 9.5 HV. The hardness of TIG welds in the weld metal zone is lower than that of MIG welds due to the greater amount of heat introduced during the welding process. The hardness of both MIG and TIG welded joints in the HAZ is higher than in the weld metal, and lower in relation to the hardness of the base metal [16,17].

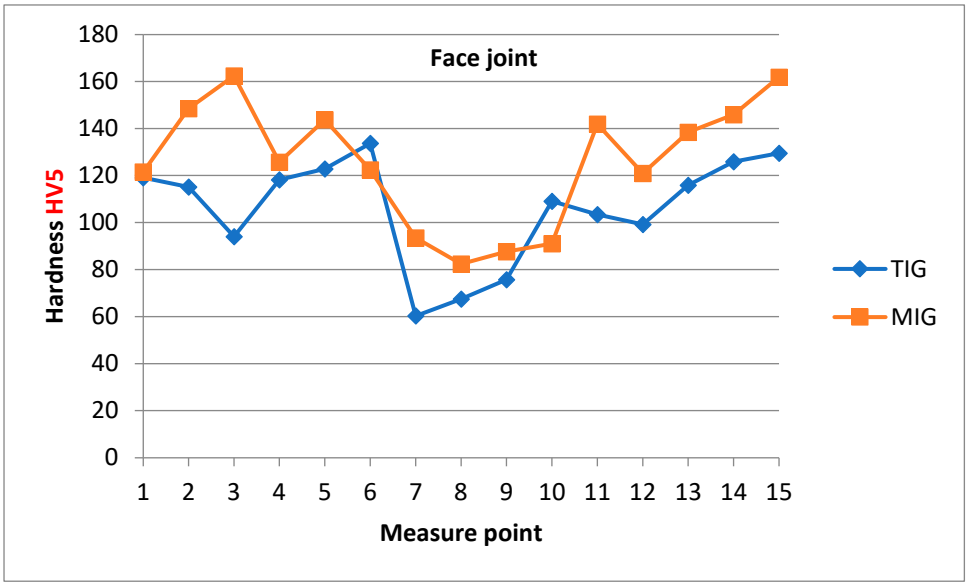

Figure 12. Hardness distribution of MIG and TIG butt joints obtained by measuring near the weld face.

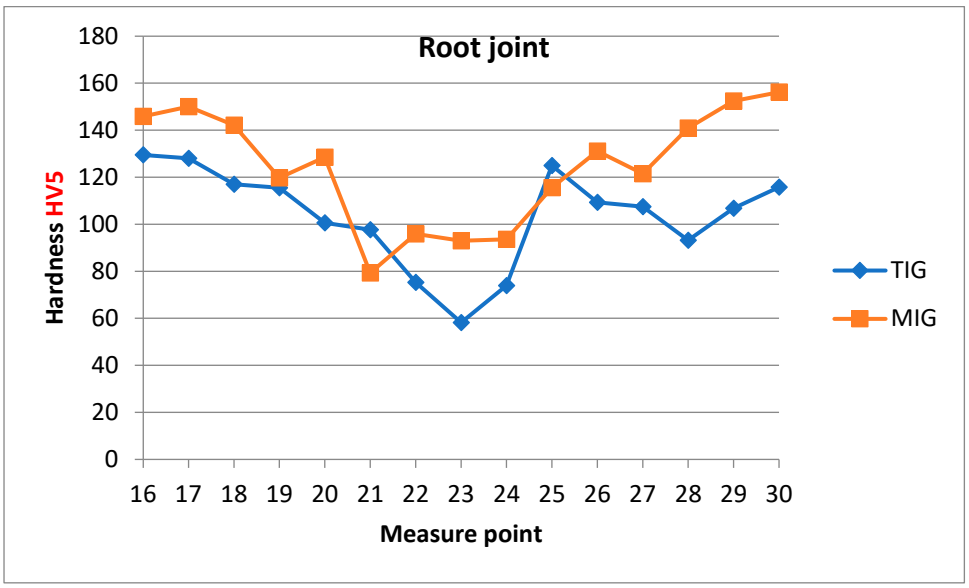

Figure 13. Hardness distribution of MIG and TIG butt joints obtained by measuring near the root of the weld.

In the FSW welded joint (Figure 14), the highest hardness due to recrystallization is in the stir zone (SZ). The lowest hardness is observed in the HAZ (about 110 HV), and then the hardness recovers in this region and increases to the level of the base metal hardness.

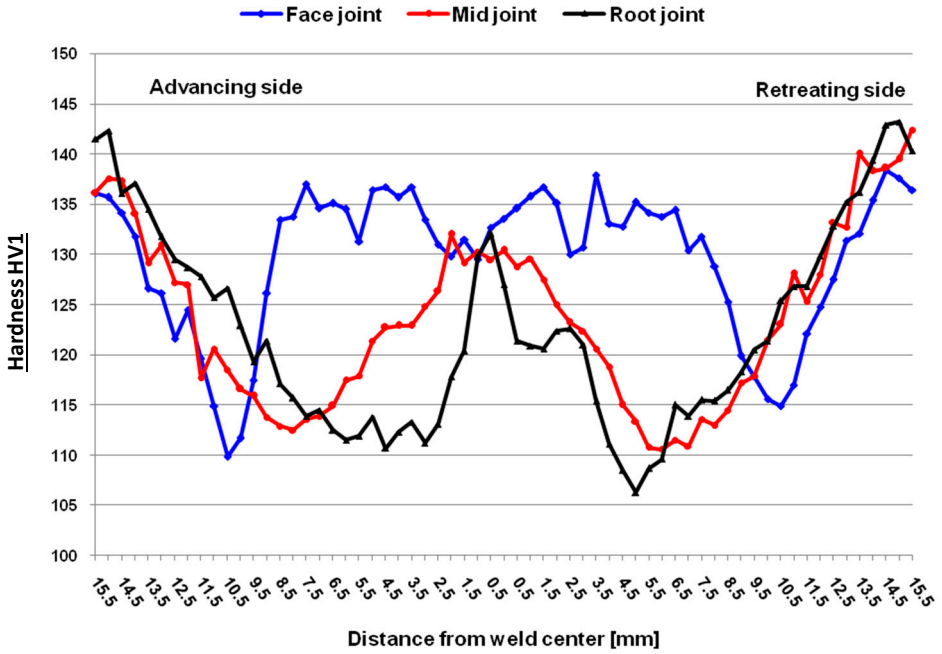

Figure 14. Hardness distribution of FSW butt joint obtained by measuring in the middle, near the face and root of the seam.

For a better understanding, a comparative graph of the hardness in the weld metal zone of MIG and TIG and in the stir zone of the FSW welding process is presented in Figure 15. The highest hardness is in the mixing zone of the FSW sample, followed by the weld metal zone of the MIG and TIG samples, respectively.

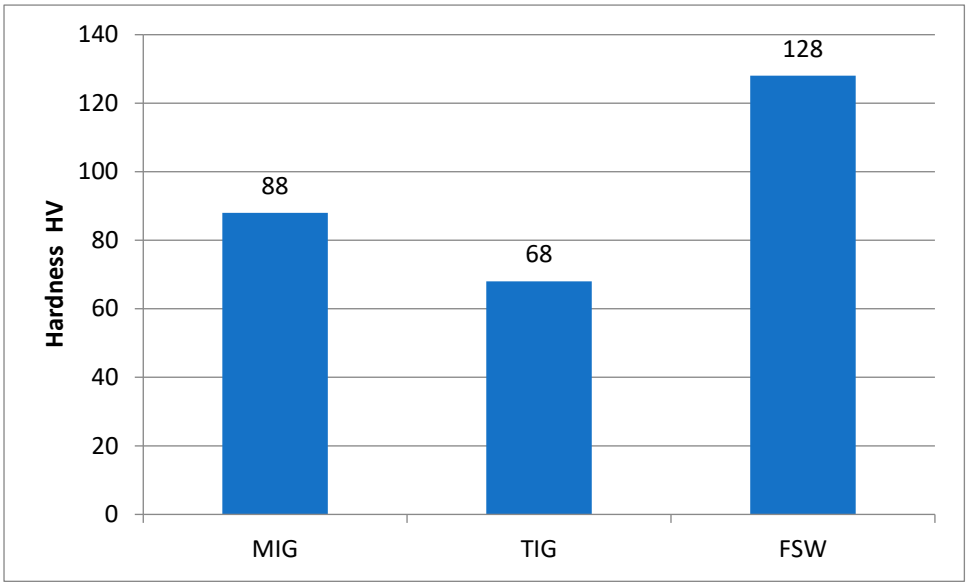

Figure 15. A comparative assessment among hardness levels at the WZ.

4. Conclusions

The influence of three joining techniques, TIG and MIG as fusion welding processes and FSW as a solid-state welding process, on the quality and properties of butt welds of aluminum alloy AA2024-T351 was investigated. Based on the test results, the following conclusions can be drawn:

1. The average hardness value for FSW joints in the stir zone is about 10% lower relative to the BM. The highest hardness is in the stir zone due to recrystallization.

2. The average hardness value of the metal weld zone for the MIG and TIG techniques using ER4043 have a lower hardness value than the heat-affected zone (HAZ) and base metal (BM) due to the differences in their main elements where the filler material ER4043 is Al-Si.
3. The ultimate tensile strength (UTS) of the FSW tensile specimen has been found to be 80% higher than that of the MIG and TIG tensile specimens.
4. FSW welds show the highest efficiency, around 97%, compared to 54% and 55% for MIG and TIG welds, respectively.
5. The place of fracture of the tensile tested specimens obtained by all welding procedures are in the weld metal for TIG and MIG welded specimens, i.e., in the stir zone for the FSW specimen.

Author Contributions: Conceptualization, D.M., M.M. and T.V.; methodology, D.M. and T.V.; validation, D.M., T.V. and D.K.; investigation, D.M. and T.V.; writing—original draft preparation, D.M. and M.M.; writing—review and editing, D.M., T.V. and D.K.; visualization, M.M., D.M. and N.Z.; supervision, N.Z., A.Đ. and D.K.; funding acquisition, D.M. and M.M. All authors have read and agreed to the published version of the manuscript.

Funding: This research was financially supported by the Ministry of Science, Technological Development and Innovation of the Republic of Serbia (Contract No. 451-03-65/2024-03).

Institutional Review Board Statement: Not applicable.

Informed Consent Statement: Not applicable.

Data Availability Statement: The original contributions presented in the study are included in the article, further inquiries can be directed to the corresponding author.

Acknowledgments: This paper is the result of research within the bilateral project with the Republic of Slovenia "Providing high reliability of aluminum structures and their parts in transport technics" in the project cycle 2020-2022 (project no. 337-00-21/2020-09/48).

Conflicts of Interest: The authors declare no conflicts of interest.

References

1. Mallick, P.K. *Materials, Design and Manufacturing for Lightweight Vehicles*; Woodhead Publishing: Sawston, UK, 2010.
2. Li, S.S.; Yue, X.; Li, Q.Y.; Peng, H.L.; Dong, B.X.; Liu, T.S.; Yang, H.Y.; Fan, J.; Shu, S.L.; Qiu, F.; et al. Development and applications of aluminum alloys for aerospace industry. *J. Mater. Res. Technol.* **2023**, *27*, 944–983. [CrossRef]
3. Lean, P.P.; Gil, L.; Ureña, A. Dissimilar welds between unreinforced AA6082 and AA6092/SiC/25p composite by pulsed-MIG arc welding using unreinforced filler alloys (Al–5Mg and Al–5Si). *J. Mater. Process. Technol.* **2003**, *143–144*, 846–850. [CrossRef]
4. Nawres, J.N. Mechanical Properties of MIG Joints for Dissimilar Aluminum Alloys (2024-T351 and 6061-T651). *Al-Khwarizmi Eng. J.* **2016**, *12*, 121–128.
5. Liamine, K.; Mohammed, E.D.; Seddik, O.; Sami, K. Dissimilar welding of aluminum alloys 2024 T3 and 7075 T6 by TIG process with double tungsten electrodes. *Int. J. Adv. Manuf. Technol.* **2022**, *118*, 937–948. [CrossRef]
6. Meshram, S.D.; Paradkar, A.G.; Reddy, G.M.; Pandey, S. Friction stir welding: An alternative to fusion welding for better stress corrosion cracking resistance of maraging steel. *J. Manuf. Process.* **2017**, *25*, 94–103. [CrossRef]
7. Prabhakar, D.A.P.; Shettigar, A.K.; Herbert, M.A.; Patel, G.C.M.; Pimenov, D.Y.; Giasin, K.; Prakash, C. A comprehensive review of friction stir techniques in structural materials and alloys: Challenges and trends. *J. Mater. Res. Technol.* **2022**, *20*, 3025–3060. [CrossRef]
8. Du, Z.; Chen, H.C.; Tan, M.J.; Bi, G.; Chua, C.K. Investigation of porosity reduction, microstructure and mechanical properties for joining of selective laser melting fabricated aluminium composite via friction stir welding. *J. Manuf. Process.* **2018**, *36*, 33–43. [CrossRef]
9. Wang, T.; Sidhar, H.; Mishra, R.S.; Hovanski, Y.; Upadhyay, P.; Carlson, B. Evaluation of intermetallic compound layer at aluminum/steel interface joined by friction stir scribe technology. *Mater. Des.* **2019**, *174*, 107795. [CrossRef]
10. Mehdi, H.; Mishra, R.S. Effect of friction stir processing on mechanical properties and heat transfer of TIG welded joint of AA6061 and AA7075. *Def. Technol.* **2021**, *17*, 715–727. [CrossRef]
11. Wang, J.; Chen, X.; Yang, L.; Zhang, G. Effect of preheat & post-weld heat treatment on the microstructure and mechanical properties of 6061-T6 aluminum alloy welded sheets. *Mater. Sci. Eng. A* **2022**, *841*, 143081. [CrossRef]
12. Kasman, Ş.; Yenier, Z. Analyzing dissimilar friction stir welding of AA5754/AA7075. *Int. J. Adv. Manuf. Technol.* **2014**, *70*, 145–156. [CrossRef]

13. Youbao, S.; Xinqi, Y.; Lei, C.; Xiaopeng, H.; Shen, Z.; Xu, Y. Defect features and mechanical properties of friction stir lap welded dissimilar AA2024–AA7075 aluminum alloy sheets. *Mater. Des.* **2014**, *55*, 9–18. [CrossRef]
14. Mastanaiah, P.; Sharma, A.R.; Madhusudhan, G. Dissimilar friction stir welds in AA2219-AA5083 aluminium alloys: Effect of process parameters on material inter-mixing, defect formation, and mechanical properties. *Trans. Indian Inst. Met.* **2016**, *69*, 1397–1415. [CrossRef]
15. Hasan, M.M.; Ishak, M.; Rejab, R. Influence of machine variables and tool profile on the tensile strength of dissimilar AA7075-AA6061 friction stir welds. *Int. J. Adv. Manuf. Technol.* **2017**, *90*, 2605–2615. [CrossRef]
16. Himanshu, L.; Paranjayee, M. Cold forming of Al-5251 and Al-6082 tailored welded blanks manufactured by laser and electron beam welding. *J. Manuf. Process.* **2021**, *68 Pt A*, 1615–1636. [CrossRef]
17. Heinz, A.; Haszler, A.; Keidel, C.; Moldenhauer, S.; Benedictus, R.; Miller, W. Recent development in aluminium alloys for aerospace applications. *Mater. Sci. Eng. A* **2000**, *280*, 102–107. [CrossRef]
18. Milčić, M.; Milčić, D.; Vuherer, T.; Radović, L.; Radisavljević, I.; Đurić, A. Influence of Welding Speed on Fracture Toughness of Friction Stir Welded AA2024-T351 Joints. *Materials* **2021**, *14*, 1561. [CrossRef]
19. Milčić, M.; Vuherer, T.; Radisavljević, I.; Milčić, D.; Kramberger, J. The influence of process parameters on the mechanical properties of friction stir welded joints of 2024 T351 aluminum alloys. *Mater. Technol.* **2019**, *53*, 771–776. [CrossRef]
20. *ISO 18273*; Welding Consumables—Wire Electrodes, Wires and Rods for Welding of Aluminium and Aluminium Alloys—Classification. ISO: Geneva, Switzerland, 2015.
21. *ASTM E8M*; Standard Test Methods for Tension Testing of Metallic Materials. ASTM: West Conshohocken, PA, USA, 2024.
22. Milčić, D.; Milčić, M.; Klobčar, D.; Đurić, A.; Zdravković, N. Structure and mechanical properties of MIG welded butt-joints of aluminum alloy 2024 T351. In Proceedings of the 16th International Conference on Accomplishments in Mechanical and Industrial Engineering DEMI 2023, Banja Luka, Bosnia and Herzegovina, 1–2 June 2023; pp. 144–150.
23. Salleh, M.N.M.; Ishak, M.; Shah, L.H.; Idris, S.R.A. The effect of ER4043 and ER5356 filler metal on welded Al 7075 by metal inert gas welding. In *WIT Transactions on the Built Environment*; WIT Press: Cambridge, MA, USA, 2016; Volume 166. [CrossRef]
24. Şik, A.; Önder, M. Comparison between mechanical properties and joint performance of AA 2024-O aluminium alloy welded by friction stir welding and TIG processes. *Kov. Mater.-Met. Mater.* **2012**, *50*, 131–137. [CrossRef]
25. Habba, M.I.A.; Alsaleh, N.A.; Badran, T.E.; El-Sayed Seleman, M.M.; Ataya, S.; El-Nikhaily, A.E.; Abdul-Latif, A.; Ahmed, M.M.Z. Comparative Study of FSW, MIG, and TIG Welding of AA5083-H111 Based on the Evaluation of Welded Joints and Economic Aspect. *Materials* **2023**, *16*, 5124. [CrossRef] [PubMed]